ACS APPLIED ELECTRONIC MATERIALS

pubs.acs.org/acsaelm Article

Laser Direct Activation of Polyimide for Selective Electroless Plating of Flexible Conductive Patterns

Jun Ren, Dongya Li, Yang Zhang,* Wenzhen Yang, Heng-yong Nie, and Yu Liu*

Cite This: ACS Appl. Electron. Mater. 2022, 4, 2191−2202 Read Online

ACCESS | Metrics & More | Article Recommendations | Supporting Information

ABSTRACT: Flexible conductive patterns on polyimide substrates are attracting increasing research interest in the areas of wearables, biomedicals, automotives, and energy harvesters. This paper reports a laser-induced selective activation (LISA) process for electroless metallization and, therefore, the creation of complex conductive patterns on polyimide substrates. In this process, a Q-switched pulsed laser is utilized for scanning the surface and forming the catalytic layer consisting of microporous structures, which enhances the stability of electroless plated metallic structures on the polyimide surface and exhibits superior mechanical stability under repeated bending and harsh environments. The high resolution of the metallic patterning enables the demonstration of a copper microgrid pattern with a line width down to 50 μm. Moreover, flexible light-emitting diode displays and electromagnetic interference shielding films are successfully manufactured to indicate the promising capability of our LISA process.

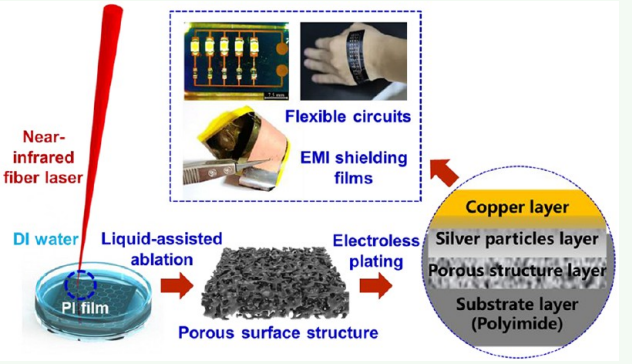

KEYWORDS: *laser-induced selective activation, microporous structure, electroless plating, polyimide, flexible electronics*

1. INTRODUCTION

Flexible conductive circuits with special deformability and conductivity are in essential demand for applications in wearable electronic devices,[1−3] medical implants,[4,5] and electromagnetic interference materials.[6,7] To fulfill the requirements of these applications, stable conductivity under various types of deformation or external stress conditions is highly desired, so a stable conductive network on a flexible polymeric insulating material as a substrate is the key. Therefore, various techniques, such as inkjet printing,[8,9] screen printing,[10] ligand-induced electroless plating,[11] and meniscus-limited electrodeposition,[12] have been investigated in the past for the construction of high-quality flexible conductive circuits. However, inkjet printing often requires a rigorous design of conductive inks, reliable nozzles, and high postprocessing temperatures, which increases the manufacturing complexity.[8,9] In comparison, screen printing seems simple and efficient, but it requires prefabricated patterned stencils, which reduces the manufacturing flexibility.[10] Ligand-induced electroless plating requires complex covalent grafting of the polymer surface.[11] Meniscus-confined electrodeposition, although allowing the fabrication of metal structures on the micro-/nanoscale through controlling the electrodeposition from microtubule ends, requires a complex electric field and low deposition rate, which restrict the capabilities for parallel manufacturing.[12]

Nowadays, burgeoning laser technology has been widely used in patterning,[13,14] surface modification,[15] medical treatment,[16] laser-assisted deposition,[17,18] and laser-induced forward transfer,[19,20] which offers new approaches for the rapid fabrication of flexible circuits.[21−23] Photolithography has therefore become the primary method used in industrial applications for etching patterns on substrate surfaces.[24] However, photolithography has inevitable disadvantages, such as being time-consuming and requiring a high capital investment and rigorous operating conditions.[24] Over the past decade, a commercially available technology, laser direct structuring (LDS), has been used to selectively deposit metal patterns by utilizing specialty plastic materials doped with laser sensitizers.[25,26] In its practice, only a portion of the laser sensitizer is utilized, which causes a huge amount of material waste, increasing cost and leading to possible heavy metal contamination.[27]

The above-mentioned issues have motivated researchers to attempt the direct deposition of metal on more general polymeric materials via laser-induced selective activation (LISA), which utilizes selective adsorption of catalytic particles on a microporous interlayer as created by liquid-assisted laser modification.[28,29] The microporous interlayer has shown the

Received: November 30, 2021
Accepted: March 21, 2022
Published: April 1, 2022

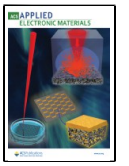

https://doi.org/10.1021/acsaelm.1c01193
ACS Appl. Electron. Mater. 2022, 4, 2191−2202

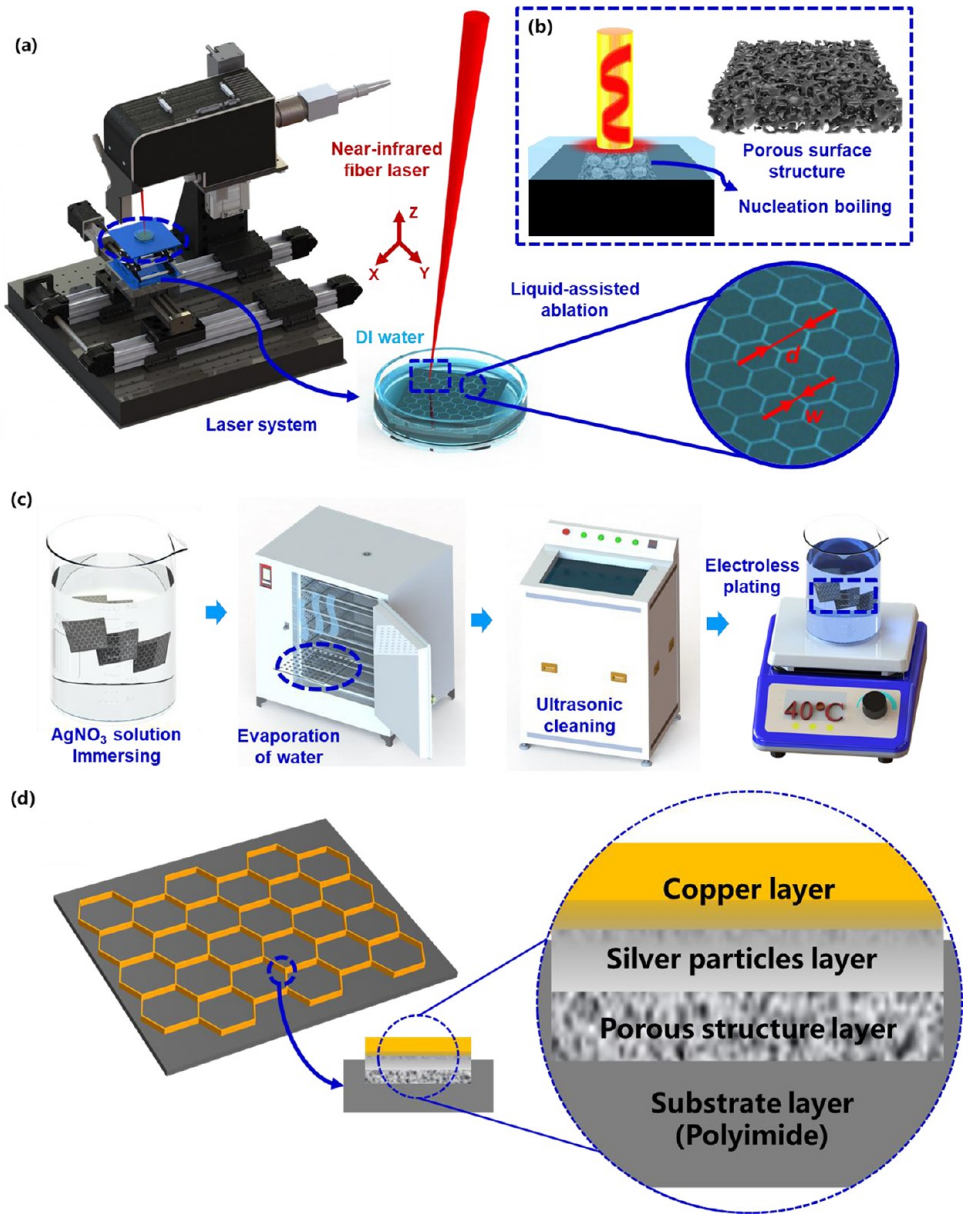

Figure 1. Schematic illustration of the fabrication process of laser-induced selective metallization on PI films through (a) liquid-assisted surface modification by laser irradiation and (c) activation of the selectively irradiated pattern via $AgNO_3$ immersion, cleaning, and electroless plating. (b) Schematic of (b) the modified PI surface and (d) the final sample with a Cu microgrid on the PI films and the composition of its cross-section.

capability for binding metallic ions and particles for electroless deposition of metals. Although the common thermoplastics are susceptible to form porous structures in LISA,[30] it is still a challenge to directly treat polyimide (PI) with high temperature resistance by the same method.[31] Due to the stable physical properties of polyimide, the researchers used alkali solution for etching and producing modified surfaces,[32] and some fascinating results have been achieved.[32,33] However, there is still an urgent need to implement a simple and precisely controlled laser-induced surface modification technique to effectively exploit the special properties of high-performance polymer-based flexible circuits.

In this paper, a facile patterned metallization process based on LISA is developed for the fabrication of microscale metallic structures on polyimide substrates. Unlike previous photolithography or LDS techniques, this work further utilized liquid-assisted laser modification for a robust mechanical anchoring of the polymer−metal layer interface. This study produces reliable conductive lines with a resistivity of less than $2.18 \times 10^{-2}\ \Omega\ \mu$m and EMI shielding effectiveness (SE) of 135 dB. Furthermore, the mechanical durability of the fabricated flexible circuit is excellent. Based on these observations, we will demonstrate the applications of the fabricated flexible circuits.

2. RESULTS AND DISCUSSION

Our proposed fabrication process for metallic micropatterns is based on LISA and is schematically illustrated in Figure 1a−c. In the typical fabrication process, a polyimide (PI) substrate is first immersed in deionized (DI) water. Subsequently, a near-infrared (NIR) fiber laser beam with a wavelength of 1064 nm is focused on the polyimide surface by a customized optical scanning system (Figure 1a). Then, the PI surface is selectively scanned and modified by liquid-assisted laser ablation (Figure 1b). Before the metallization, the laser-modified substrate is

https://doi.org/10.1021/acsaelm.1c01193
ACS Appl. Electron. Mater. 2022, 4, 2191−2202

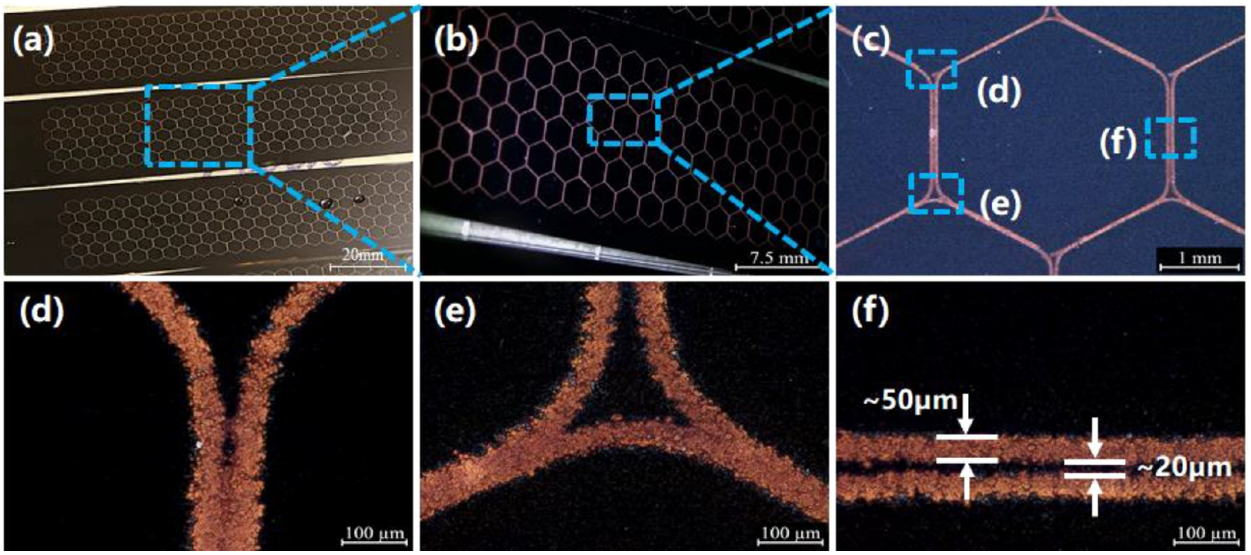

Figure 2. Optical images of samples with copper patterns. Three samples with hexagonal patterns (a) and an enlarged view (b). Particular locations of a hexagon (c) from the pattern in part b are shown in parts d–f. Note that the image in part f was rotated 90° compared to that in part c. The two parallel lines in part f are 50 μm wide and separated.

activated in a silver nitrate solution for 10 min, by which the silver ions diffuse onto the PI surface. The activated sample is then heat-dried and ultrasonically cleaned to remove the silver ions on the nonmodified area of the PI film (Figure 1c).

During the following electroless copper plating (ECP) at 40 °C, the copper atoms are selectively deposited on the Ag-activated surface to form a uniform metallic pattern in the ECP bath (Figure S1, Supporting Information). Again, the film is rinsed in DI water to remove the residual ECP solution, and a flexible PI film with a patterned Cu microgrid is obtained as shown in Figure 1d. The entire fabrication process is solution-based, performed in the ambient environment, and suitable for large-area fabrication.

Flexible PI films with a copper microgrid were fabricated for testing the accuracy of our LISA process. As displayed in Figure 2a,b, the new process can successfully produce continuous and complex features of the prototyped Cu microgrid with high resolution. The enlarged views in Figure 2d–f show that the line width of the copper lines can be controlled to less than 50 μm, which was limited by the laser spot size of ~50 μm in this study. The minimum distance between two adjacent conducting lines was ~20 μm in this study as determined by the positioning accuracy of the belt-based linear stages as used in our setup.

The selective electroless copper deposition was validated by an EDS (energy-dispersive X-ray spectroscopy) analysis of the as-fabricated microgrids. The compositions of PI surfaces before and after ECP were analyzed. As seen in Figure 3a,b, the compositions of the PI surface before ECP were 76.06 wt % C, 23.82 wt % O, and 0.12 wt % other elements (N), and the compositions of the PI surface after ECP were 99.94 wt % Cu and 0.06 wt % other elements. It can be seen in Figure 3b that only the Cu element was detected, and the C–O–N element disappeared, which can be explained by the fact that the Cu metal layer was sufficiently thick, or the PI surface was completely covered by a uniformly, densely deposited Cu layer.

It should be noted that the black polyimide films were used as substrates in this study because of their high absorption (almost 100%) of light at the wavelength of 1064 nm (in Figure 3c). The high absorption can help obtain the porous surface structure at a lower laser power. More importantly, since we operated the LISA in water, the black color design was beneficial for suppressing the noise effects from ambient lights. In practice, LISA has also been considerably applied to other melanocratic polymers, such as polycarbonate (PC), epoxy glass fiber substrate with flame resistance grade 4 (FR4), acrylonitrile butadiene styrene (ABS), and polybutylene terephthalate/polyethylene terephthalate (PBT/PET).[30]

The fabrication process was then investigated by varying the laser scanning cycles N_{scan}, while the other parameters (laser power and pulse frequency) were maintained. As shown in Figure 4a, five groups of samples were fabricated by laser irradiation for 1–5 cycles, separately. The effective spot of irradiation could not completely modify the original PI surface with only less than three cycles of laser irradiation. After the ECP process, as shown in Figure 4b, many defects were left on the processed PI surface that was irradiated for 1 or 2 cycles. Therefore, a sufficient dosage such as at least three cycles of laser irradiation was necessary to fulfill the completeness of the laser energy distribution. A fully metallized surface could be obtained only after more than three cycles of laser irradiation. As shown in Figure 4c, the sheet resistance can be controlled below 0.3 Ω/sq after more than 3 cycles of laser irradiation.

The fabricated copper layer after 30 min of ECP is relatively thin (~0.5 μm) (Figure 4f), and the electric resistivity ρ of the copper layer is only about 0.15 Ω μm. By increasing the electroless plating time and therefore the density and thickness of the copper layer, the results shown in Figure 4d show that after 60 min the resistivity remained constant, and the copper layer was densely formed on the surface area after laser processing, which can be confirmed in the optical images as in Figure 4e. Based on the morphology observation and the resistance measurement, the electroless plating time of 60 min was selected for subsequent experiments.

To prove the advantage of the current work, we compare the sheet resistance, metal thickness, and resistivity of the LISA-based flexible circuits with other fabrication techniques from the literature, as shown in Table 1. This clearly shows that the LISA-based flexible circuits fabricated in the current work deliver one

https://doi.org/10.1021/acsaelm.1c01193
ACS Appl. Electron. Mater. 2022, 4, 2191–2202

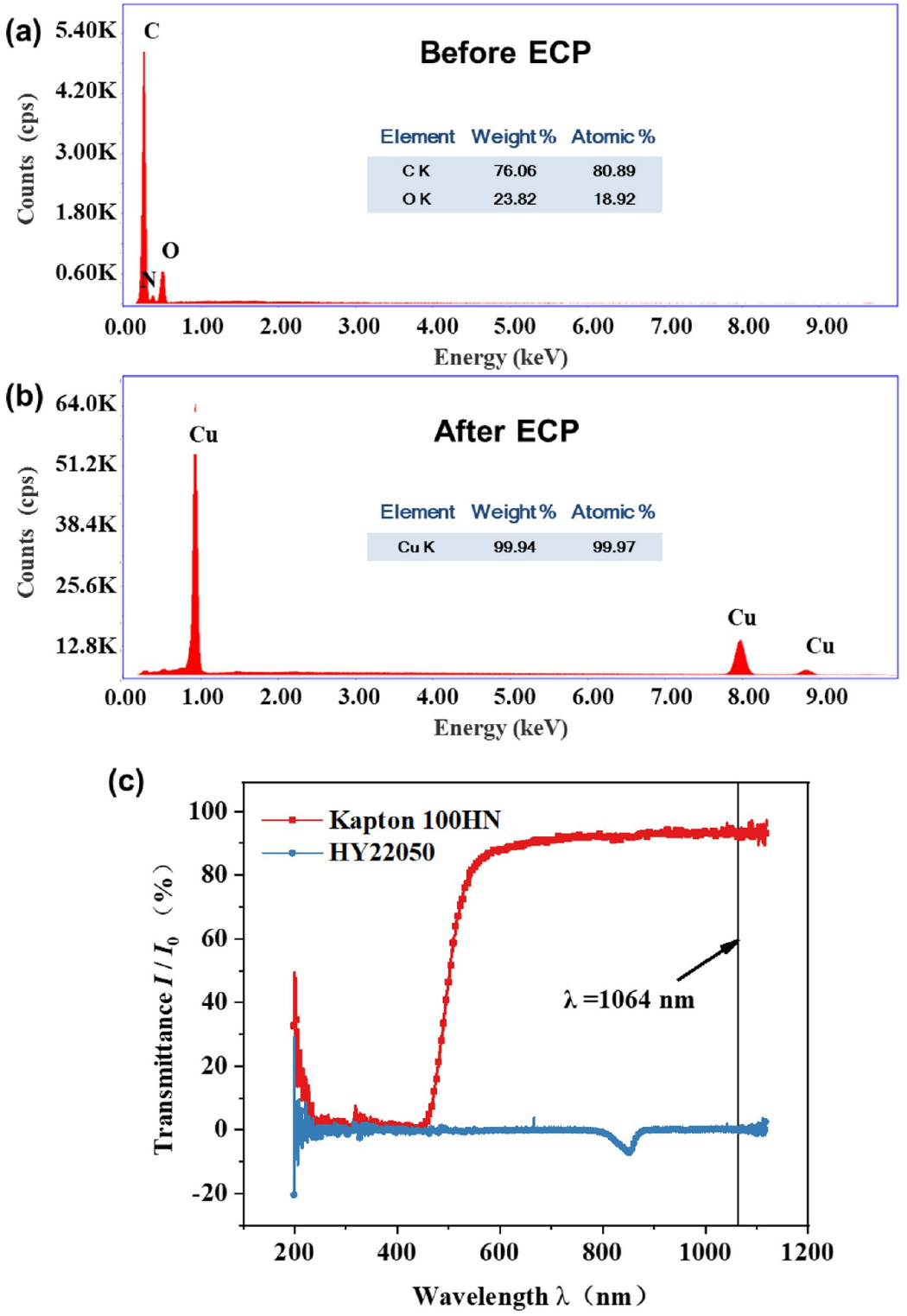

Figure 3. EDS spectra of the polyimide before (a) and after (b) electroless copper plating. (c) Transmittance spectra of black PI (HY22050) from Runhai Electronics Co. Ltd. and sandy brown PI (Kapton 100HN) from Du Pont-Toray Co. Ltd. in the region 200−1100 nm.

of the lowest resistivity values compared with other fabrication techniques, proving the advantage of this work in the application of flexible electronics.

The possible mechanism of the selective metallization of PI was further studied. The LISA process is usually implemented on other polymers in a water medium,[28−30,40−42] which indicates that the laser process at the interface between water and PI is significant for an effective modified surface. By comparing the surface morphology of PI after laser irradiation in water and in air, the mechanism of laser modification at the interface could be speculated. As shown in Figure 5a, the PI was laser-irradiated in air, and macropores were formed. The diameter of each pore is about 30 μm, showing agreement with the theoretical diameter of the laser spot. After the ECP

https://doi.org/10.1021/acsaelm.1c01193
ACS Appl. Electron. Mater. 2022, 4, 2191−2202

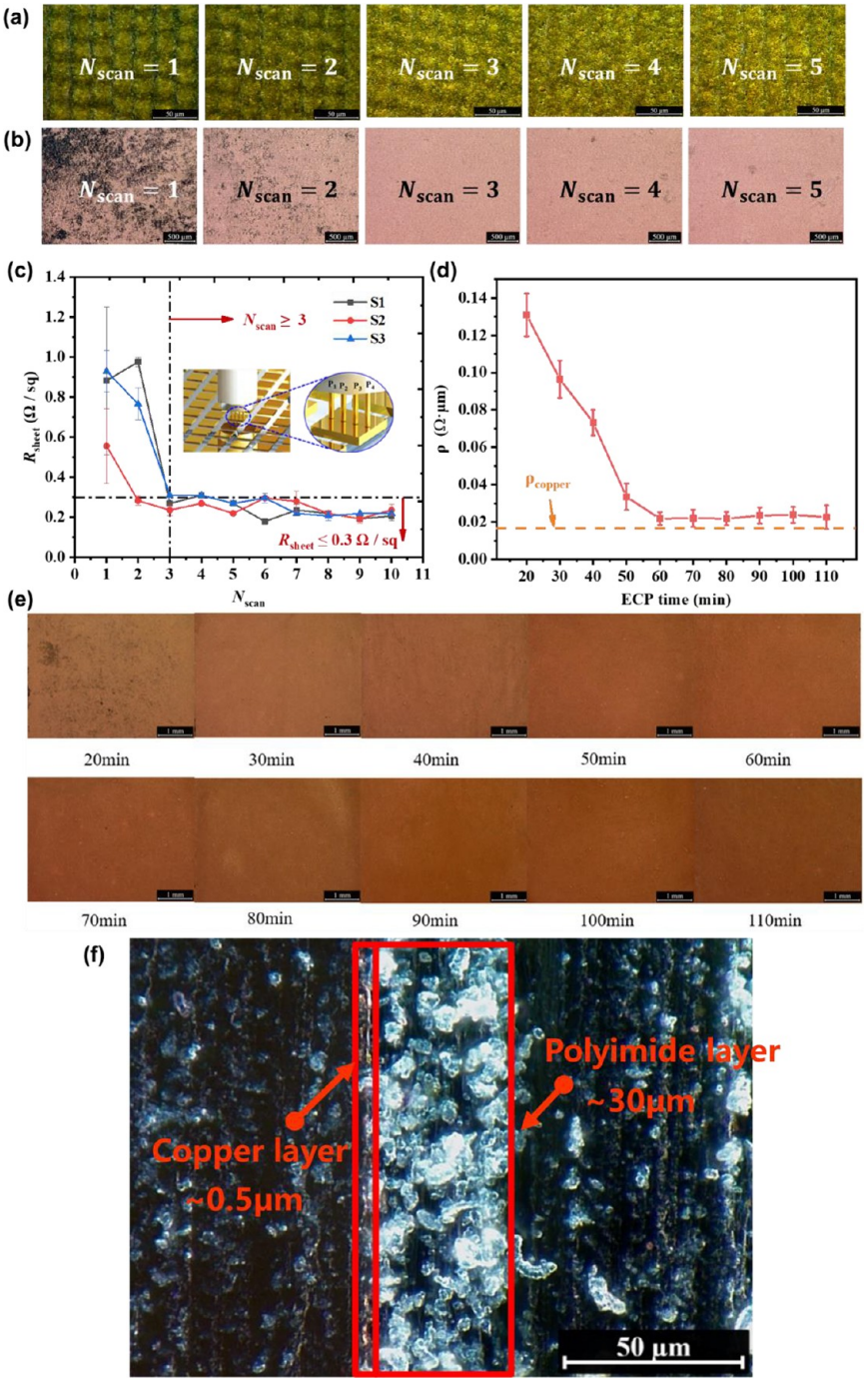

Figure 4. Optical images of the laser-modified PI (a) and the metallized layer after different scanning times (b). The sheet resistance values corresponding to the samples in part b are plotted in part c. Resistivity (d) and corresponding optical images (e) of the samples with different ECP durations. (f) Cross-sectional view of the interface between the copper and PI layers.

process, as presented in Figure 5b, the copper grows along the irregular shape of the pore structure, forming an irregular metal cover over the pore structure. The macropores may reduce the adsorption ability of the activation solution, resulting in the loss of the activation seeds in the ultrasonic cleaning step and uneven copper deposition in the ECP step.

In contrast, when laser modification was carried out in water, microporous structures were formed as shown in Figure 5c, which could contribute to retaining the activation solution and achieving a more uniform copper deposition (Figure 5d). The reason that microporous structures were formed in the water is supposed to be the nucleate boiling at the interface between water and the PI surface.[43,44] At atmospheric pressure, nucleate boiling occurs when the excess temperature of water exceeds 5−30 °C. Maintaining the surface temperature requires controlling the heat flux within a certain range.[45,46] In this case, the temperature of the polymer surface rose rapidly, and there was local area transfer to the glassy state or molten state, which was prone to deformation[47] and formed a local microcrack as a nucleation center for nucleate boiling. Taking the nucleation center as the starting point, water changes from liquid phase to gas phase, and the resultant bubble grows and separates. After

https://doi.org/10.1021/acsaelm.1c01193
ACS Appl. Electron. Mater. 2022, 4, 2191−2202

Table 1. Comparison of Resistivity of Flexible Circuits between the LISA Process and Other Techniques

material	fabrication technique	R_{sheet} (Ω/sq)	t_{metal} (μm)	ρ (Ω μm)	ref
copper/Ag layer on PET/PI	patterning of silver nitrate inks and ECP		0.3	2.08×10^{-2} (119% Cu)	34
copper layer on PET	printing of Cu NPs and ECP	0.006	0.2465	2.01×10^{-2} (118% Cu)	35
copper/Pd layer on PI	spin-coating of Pd complex ink and ELD	0.034	4	13.6×10^{-2} (777% Cu)	36
copper layer on PEEK/CNT composites	$NaBH_4$/NaOH solution immersing and ECP	0.015	9	13.5×10^{-2} (771% Cu)	37
copper/Ag layer on PET	SiO_2/Ag liquid modification and ECP		2.4	8.6×10^{-2} (491% Cu)	38
copper layer on PET	MPTES modification and ECP	0.054	1	5.43×10^{-2} (310% Cu)	39
copper/Ag layer on PI film	LISA and ECP for 20 min	0.252	0.52	13.1×10^{-2} (748% Cu)	this work
copper/Ag layer on PI film	LISA and ECP for 40 min	0.103	0.71	7.32×10^{-2} (418% Cu)	this work
copper/Ag layer on PI film	LISA and ECP for 60 min	0.023	0.96	2.18×10^{-2} (124% Cu)	this work
copper/Ag layer on PI film	LISA and ECP for 110 min	0.022	1.18	2.26×10^{-2} (129% Cu)	this work
				1.75×10^{-2}	bulk copper

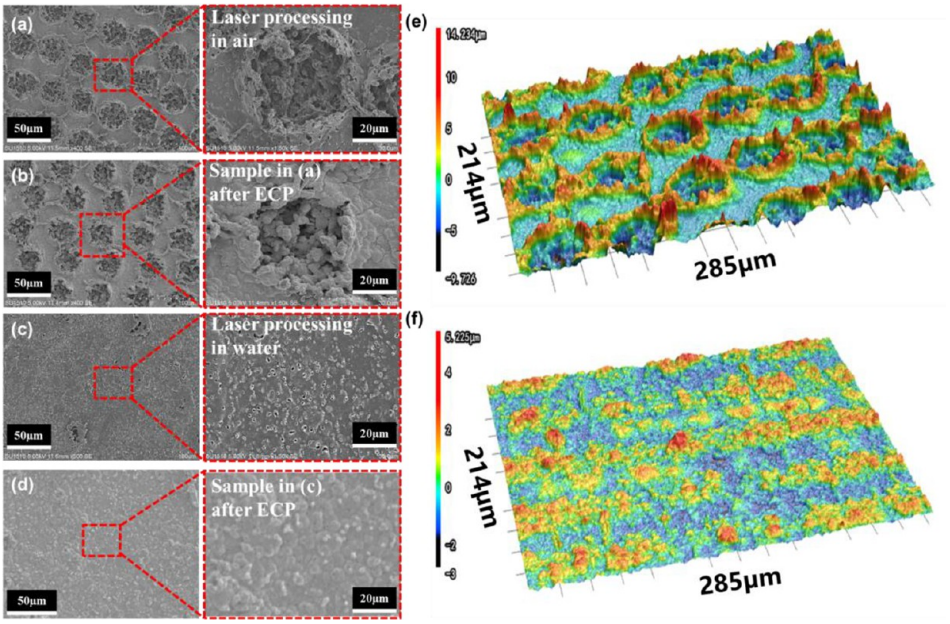

Figure 5. SEM images of a laser-modified PI surface (a) in air and (c) in water. The SEM images of the samples in parts a and c after ECP are shown in parts b and d, respectively. The surface morphology of the PI substrate after the laser processing (e) in air and (f) in water is obtained using a laser scanning confocal microscope.

bubble separation, the surrounding low-temperature liquid quickly flows in to fill the generated cavity and rapidly solidifies the molten surface, and then, a porous morphology is formed. According to the measurements using confocal microscopy, the average surface roughnesses of the PI substrates processed in air and in water were 2.4 μm (Figure 5e) and 0.9 μm (Figure 5f), respectively. Based on the van Oss et al. acid/base theory, the microporous structure allows for greater surface tension and interfacial work, thus retaining the activation solution for allowing the silver ions to be activation seeds.[29] Accordingly, ECP only occurs in the laser processing area because the porous structure with the remaining activation solution allows the catalytic reduction deposition reaction to occur. In addition, it was noted from Figure 5f that the maximum roughness for PI film after LISA in water was about 5.225 μm, which was just the effective thickness of the porous structure and therefore the minimum required thickness of the PI film. In fact, the thickness of the commercial PI film used in our study was about 30 μm, much larger than this effective thickness of the porous structure.

The adhesion strength of the metal layer on the substrate was confirmed by a tape test according to the standard test method (D3359-09, American Society of Testing Method).[48] As shown in Figure 6a, a metallized sample of 20 mm × 20 mm was prepared. Then, the metal layer was cut into 10 × 10 grids (Figure 6b). The pressure-sensitive tape was pasted on the metal layer and then peeled off from the copper surface. As presented in Figure 6c, 0−5% of the deposited copper came out after the peel test. The edge of each metal layer cell is neat, and no cell is stripped. The adhesion between the copper layer and the PI film belongs to class 5B according to ASTM-D3359. That means that the adhesive strength achieves the highest grade of the standard. The porous structures of the laser-modified PI surface form a mechanical anchorage with the deposited copper crystal; thus, the Cu layers are tightly bonded to the substrate through the porous structures. Compared with chemical-bond-based methods, the LISA process that creates a mechanical anchorage is a more facile method without using extra chemical reagent.

The excellent adhesive performance of the metal layer greatly enhances the stability of the plated metal layer under bending, heating, or chemical attack. The electrical conductivity of the metalized layer under cyclical bending was examined. Figure S2 in the Supporting Information presents the customized cyclical bending testing system. The sheet resistance of metalized surfaces was collected based on a customized high-throughput

https://doi.org/10.1021/acsaelm.1c01193
ACS Appl. Electron. Mater. 2022, 4, 2191−2202

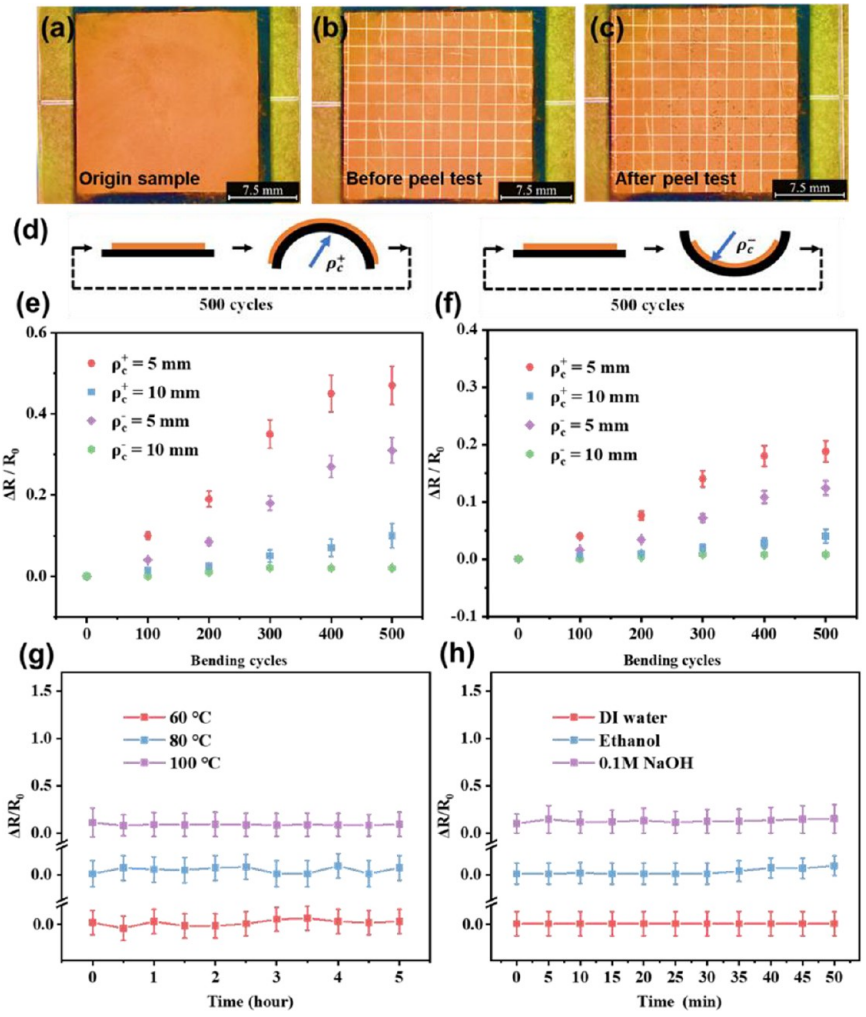

Figure 6. Optical images of (a) a square sample (20 mm × 20 mm) of a copper layer deposited on a PI substrate and the sample being cut to 10 × 10 grids before (b) and after (c) the peel test using a scotch tape. (d) Schematic diagram of the cyclic bending test of two types of bending states. Resistance variations corresponding to samples after 30 min of ECP (e) and after 60 min of ECP (f). The sheet resistance variations of the copper layer under heating and chemical attack are shown in parts g and h, respectively.

resistance meter (Figure S3, Supporting Information).[49] As shown in Figure 6d, ρ_c^+ and ρ_c^- are the curvature radii of the sample when bending inward and outward, respectively. A series of cyclical bending tests were conducted on the PI substrates with the as-fabricated copper layer. The specimens used in these tests were fabricated in the same way except for the ECP time. The specimens were divided into 2 groups. Each group was bent 500 times at radii of 10 and 5 mm, separately. The ΔR and R_0, representing the resistance change for the bent and the initial states, respectively, were recorded every 100 times and plotted in Figure 6e,f in the form of the ratio of ΔR to R_0. This shows that the resistance of the copper layer barely changed even after 500 bending cycles when the radius of curvature was 10 mm. When the radius of curvature was 5 mm, obvious changes were observed in the resistance of specimens with 30 min of ECP time. The electrical conductivity reduced by approximately 50%, which is not satisfactory for general applications. However, the electrical conductivity of the metallic copper layer with 60 min of ECP time after 500 cycles of outward bending only reduced by ~18%. Meanwhile, after 500 cycles of inward bending, the electrical conductivity of the metallic copper layer reduced by ~11%, which meets the requirements of most flexible electronics applications. These results show a realistic potential of the metallized PI developed here for consumer applications based on flexible electronics. There are two possible reasons for the rise of resistance: during the movement cycle, the contact between the test fixture and copper slips slightly, resulting in the increase of contact resistance;[50] and the higher increases in the resistance values arise because of copper layer cracking under larger strains.[51]

The environmental stability of the as-fabricated PI-based flexible electrode was evaluated by exposing the sample to elevated temperatures and dipping them in ethanol, DI water, and 0.1 mol/L sodium hydroxide solution (pH = 14). The purpose of setting three liquids is to test the tolerance of samples in organic, neutral, and highly alkaline environments. Figure 6g shows that, after the heating at 60, 80, and 100 °C for 5 h, the sheet resistances of the copper layer remained unchanged. Figure 6h shows that, after immersion in those liquid environments for 50 min, no noticeable changes in the sheet resistances of the electrode were observed. Although copper and PI are resistant to organic solvents and alkaline environments, the superior stability of the PI-based flexible electrode is attributed to the excellent adhesion of the mechanical anchorage.

https://doi.org/10.1021/acsaelm.1c01193
ACS Appl. Electron. Mater. 2022, 4, 2191−2202

The first demonstration of the proposed methodology is shown in Figure 7a, wherein the surface mounted device (SMD)

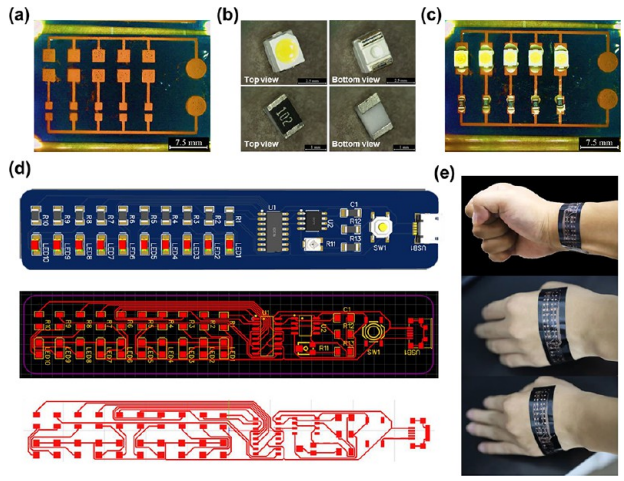

Figure 7. Optical images of a circuit pattern of an electroless plated copper layer on laser-modified PI substrate (in water) (a), SMD package devices of a light-emitting diode (upper row) and a resistor (lower row) (b), and the final flexible circuit board on which light-emitting diodes and resistors are soldered (c). (d) Typical conventional rigid circuit board, printed circuit board design, and its circuit trajectory. (e) The fabricated flexible circuits were conformally attached to the human skin.

circuit, fabricated via LISA and ECP on a PI substrate, has five parallel patterns for housing devices, with the lines being 20 mm long and 0.5 mm wide. The pads (Figure 7b) are for connecting the five light-emitting diodes and five resistors shown in the upper and lower rows, respectively. As shown in Figure 7c, the chip resistors were pasted onto the circuit as current limiting resistors, and the conductive silver pulp was used as an interconnect to bridge the resistor components and the solder pads on the circuit. Finally, the chip light-emitting diodes were mounted onto the solder pads with the conductive silver pulp. A video of the working devices and circuits is shown in Movie S1 (Supporting Information). Figure 7d shows a typical conventional rigid circuit board, the printed circuit board (PCB) design, and its circuit trajectory. This PCB design contains a CD4017 integrated circuit (IC) chip, an NE555 IC chip, and other devices. The NE555 provides a periodic square-wave signal to the CD4017, which circulates this signal in turn to 10 groups of LEDs and current limiting resistors. A working video of the designed circuits is shown in Movie S2 (Supporting Information). As demonstrated in Figure 7e, the flexible circuit was fabricated on PI surfaces via LISA and ECP and then conformally attached to the human skin. The fabrication process is shown in Movie S3 (Supporting Information) for a demonstration of the rapid digital manufacturing capability. In summary, the metallized PI surface fabricated by LISA and ECP is practical for flexible electronic circuits.

Metals such as copper and aluminum are commonly used as electromagnetic shielding materials. Still, their poor flexibility and high density make it difficult to meet the requirements of lighter and more flexible electromagnetic shielding materials for the next generation of portable and wearable smart electronic products. Therefore, electromagnetic interference (EMI) films prepared by the surface metallization process have the characteristics of light weight and good flexibility. The ability of surface conformation and electromagnetic interference shielding performance can be used as an ideal substitute for metal shielding materials. The flexible EMI shielding films, prepared by the LISA process, are shown in Figure 8a and could be bent at a large curvature for being conformally pasted to any free-form surfaces. The EMI shielding performance was further investigated. As shown in Figure 8b, four PI films were laser-modified at different laser pulse frequencies (f_{rep}) of 30−60 kHz and then metallized by the same ECP process. Figure 8c reveals that the copper on the PI surface had different degrees of uniformity because of the different laser energy distribution. The EMI shielding performance is shown in Figure 8d; the total shielding efficiency (SE_T) was relatively low (~60 dB) when f_{rep} was 30 kHz. With the increase in f_{rep}, the total shielding efficiency increases continuously. When f_{rep} is 60 kHz, SE_T is ~140 dB, which is close to that of the copper foil. Theoretically, the EMI shielding effectiveness can be evaluated according to the following formula, including reflection loss SE_R and absorption loss SE_A. SE_A and SE_R are both proportional to the conductivity of the shielding material.[52,53] The improvement in electrical conductivity can promote the EMI shielding efficiency. Therefore, the reason that the increase in f_{rep} improves SE_T is supposed to be the high conductivity of the deposited copper layer under relatively higher f_{rep}. According to the above data, the LISA film possesses high EMI shielding efficiency in the original state. In order to further verify that the LISA film can still maintain effective EMI shielding efficiency under conformal working conditions, the SE_T under bending conditions was tested and compared with the data of the copper foil. As presented in Figure 8e, in the curved state, the SE_T of both LISA films and copper foil can decrease significantly relative to the original data. However, the SE_T of the LISA film was slightly higher than that of copper foil, which can maintain a practically effective EMI shielding ability (~50 dB), both in the inward bending state and outward bending state. The better performance of LISA films may be due to the mechanical anchoring of the copper layer and PI, which improves the toughness of the overall film. Thus, compared with copper foil, LISA films can maintain good electrical conductivity under bending damage.

3. CONCLUSION

In summary, based on LISA technology, we have developed a facile electroless metallization process of microscale metallic structures on PI substrates for flexible electronic applications. This process utilizes the laser modification of PI surfaces and the selective adsorption of catalytic silver ions on porous modified surfaces, enabling the electroless metallization on the PI substrates. Using this method, a copper microgrid pattern with a line width down to 50 μm was successfully demonstrated. Moreover, the superior stability of the deposited copper layer and PI substrate enable the level-5B adhesion strength and the resistivity of less than 2.18×10^{-2} Ω μm under repeated bending and harsh environments. Versatile electronic applications, including SMD circuits and EMI films, were successfully demonstrated on flexible polyimide substrates using this method. Because of the strong adhesion of the mechanical anchorage of porous interlayers, excellent mechanical, electrical, and thermal stabilities of the metallic structures were observed on the fabricated devices. With the unique performance of a high-throughput, low-cost, pretreatment-free, and high-resolution fabrication compared with the current conventional approaches in the electronics industry, this process has a broad application in the field of flexible electronics manufacturing.

https://doi.org/10.1021/acsaelm.1c01193
ACS Appl. Electron. Mater. 2022, 4, 2191−2202

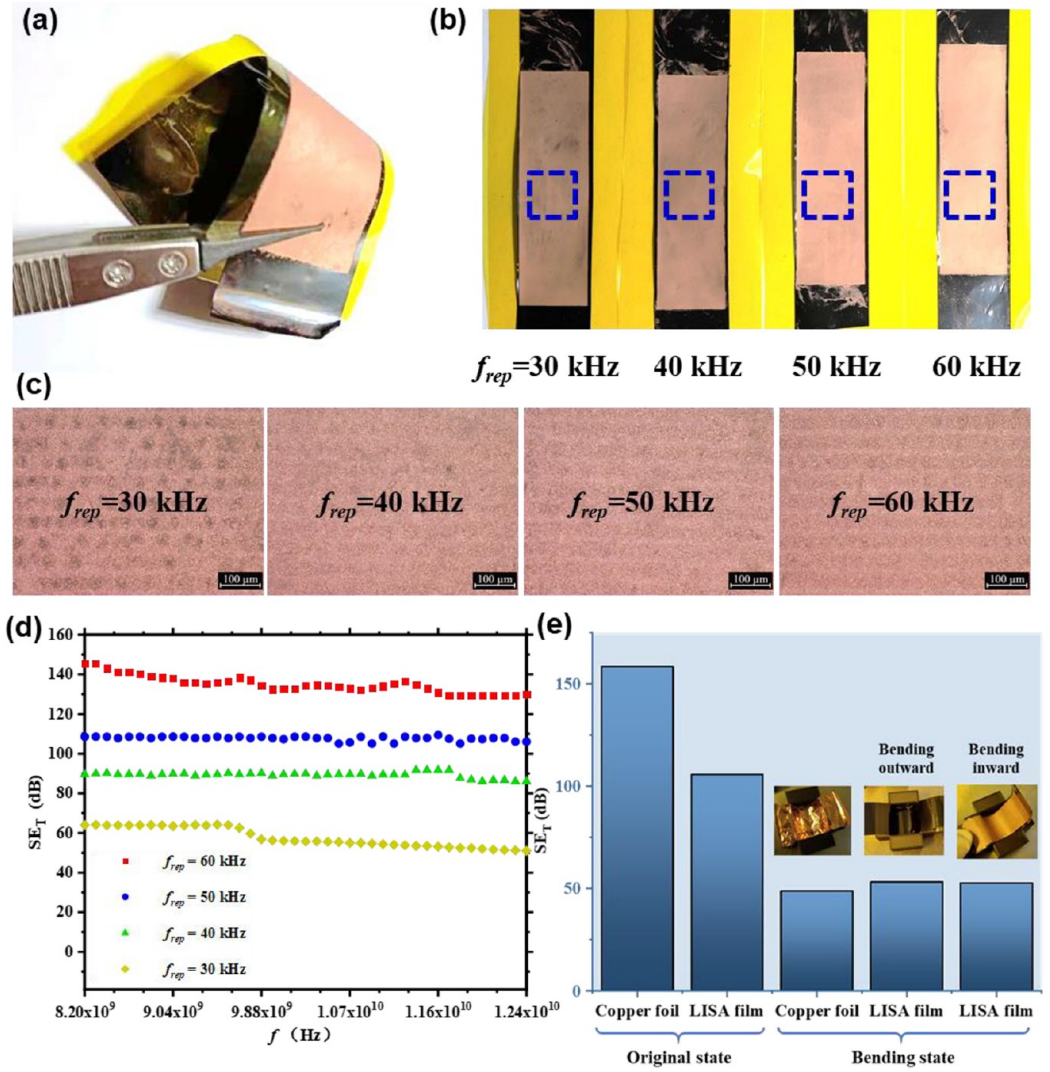

Figure 8. Optical images of EMI shielding films (a) and four others processed in different repetition frequencies (b). The enlarged view of samples in part b is shown in part c. (d) Plot of SE_T results of LISA films with a different pulse frequency in the laser irradiation process. (e) Plot of SE_T results of LISA films and copper foils in the original state and in the bending state.

4. MATERIALS AND METHODS

Materials Preparation. PI films were purchased from Runhai Electronics (Shenzhen, China). Silver nitrate, copper sulfate pentahydrate, sodium hydroxide, and formaldehyde aqueous solution (37%) were all analytical reagent (AR) grade and purchased from Sinopharm Chemical Reagent (Shanghai, China). AR-grade ethylenediaminetetraacetic acid disodium salt dihydrate was purchased from Macklin Biochemical (Shanghai, China), and potassium sodium tartrate was from Titan Technology (Shanghai, China). Different from our previous research work, the activation solution was prepared by dissolving 16.9 g/L silver nitrates in deionized (DI) water, which replaced the expensive, previously used Pd/Sn as the catalyst for ECP. An ECP bath was prepared by dissolving 21 g of ethylenediaminetetraacetic acid disodium salt dihydrate and 16 g of potassium sodium tartrate in 1 L of DI water. Then, 12 g of copper sulfate pentahydrate and 15 g of sodium hydroxide were added stepwise until a homogeneous solution was formed (Solution A). Formaldehyde aqueous solution (15 mL) was sucked into a dropper (Solution B) and was added dropwise into Solution A at a rate of 5 mL/min under stirring for about 10 min.

Set-Up of the Laser Scanning System. A Q-switched near-infrared (NIR) pulsed fiber laser (WF-LD20, Woofee Laser Tech) was equipped with a customized optical scanning system (Figure S4, Supporting Information). The NIR laser wavelength is 1064 nm with a pulse duration of 100 ns. The laser beam was focused on the surface of the substrate through a digital galvanometer scanner (F10, Feeltek Laser Tech). A compact laser displacement sensor (HL-G105-S-J, Panasonic) with a resolution of 1.5 μm was aligned at the head of the galvanometer scanner for in situ measuring the distance from the galvanometer scanner to the substrate surface. An external Z-axis linear actuator (EZS4E010-A, Oriental Motor) was equipped to adjust the galvanometer's height, which ensures that the surfaces of different samples were aligned within the same focal plane at f = 144 mm. A transparent dish containing DI water is placed on an XY stage (W40-10, CCM) to adjust the samples' position in the plane.

Manufacturing of Metallic PI Films. PI films were first cleaned in ethanol and DI water in an ultrasonic bath. After being dipped into the transparent dish of the laser system, the films were selectively scanned by NIR laser to generate porous structures on their surfaces. The laser parameters used are as follows: the average power is 2 W, the pulse frequency 40 kHz, and the scanning speed 1500 mm/s. Thereafter, PI films were transferred from the dish. After rinsing with DI water to remove the ablation ash, the samples were dried under nitrogen flow. The laser-modified PI films were first immersed in the activation bath at 40 °C for 10 min. Then, the samples were heat-dried in an oven at 50 °C for 5 min. Thereafter, the activated films were ultrasonically cleaned in DI water for 20 s to remove the residual silver nitrate in the unmodified area. Subsequently, the PI films were immersed in the ECP bath at 40 °C for 60 min, where copper ions were reduced by formaldehyde and

https://doi.org/10.1021/acsaelm.1c01193
ACS Appl. Electron. Mater. 2022, 4, 2191−2202

deposited on the activated areas of PI substrate. Afterward, the samples were rinsed in DI water and dried under a nitrogen flow.

Applications. The five-parallel circuitry patterns were created on the PI films through selective laser modification. Then, the patterned samples were activated by silver nitrates and then immersed in the ECP bath for 60 min for the metallization. Subsequently, LEDs and resistors were welded on the circuits using silver paste. Finally, the fabricated flexible LED displays were connected to an external control circuit with a programmed microprocessor. Rectangle patterns were created on the PI films through selective laser modification at the laser pulse frequency from 30 to 60 kHz. Then, the patterned samples were activated by silver nitrates and then immersed in the ECP bath for 60 min for the metallization. Subsequently, another piece of PI film was pasted onto the metallized surface for insulation. Finally, the fabricated flexible EMI shielding films can be conformally pasted onto any free-form surface of items that need to be protected from electromagnetic radiation.

Characterizations. The morphologies were characterized using scanning electron microscopes (SU1510, Hitachi, Japan; TM3030, Hitachi) and an optical microscope (DVM6, Leica). Confocal laser scanning microscopy (VK-X1050, Keyence) was used to measure the surface roughness (S_a) under a laser mode with a scanning size of 285 × 214 μm^2. The compositional analysis was performed by energy-dispersive X-ray spectroscopy (EDS, EDAX Instruments) as an attachment on a scanning electron microscope with an accelerating voltage of 30 kV. The sheet resistances of the plated conductive patterns were measured by using a customized four-probe method. During the measurement, four probes were placed on the center of a square sample, and the resistance was recorded with a source meter (2400, Keithley). During the measurement for the repetitive bending or stretching process, the sample was fixed to a home-built moving stage, and the resistance was recorded with an LCR meter (E4980A, Keysight). The adhesive strength was measured using a transparent tape (Scotch 6001, 3M) according to the testing standard of ASTM-D3359. Optical transmission spectra were recorded using a spectrometer (HR2000+, Ocean Optics). The EMI shielding performances of samples were measured using a vector network analyzer (E5063A, Keysight). The samples were sandwiched in the middle of a two port system and were in turn connected to the vector network analyzer. The microwave scattering parameters, including S11 and S21, were then recorded in the X-band frequency range. The shielding effectiveness by absorption SE_A, the reflection SE_R, and the total shielding effectiveness SE_T were calculated based on the measured microwave scattering parameters.

■ ASSOCIATED CONTENT

Supporting Information

The Supporting Information is available free of charge at https://pubs.acs.org/doi/10.1021/acsaelm.1c01193.

Schematics of the electroless copper plating process; photographs of the customized cyclical bending testing system; schematics and photographs of the customized high-throughput resistance meter; and photographs of the laser scanning system (PDF)

Movie S1: Demonstration of the working devices and circuits (MP4)

Movie S2: Demonstration of the designed circuits (MP4)

Movie S3: Real-time fabrication process (MP4)

■ AUTHOR INFORMATION

Corresponding Authors

Yang Zhang − *Department of Mechanical Engineering, Technical University of Denmark, 2800 Lyngby, Denmark*; Email: yazh@dtu.edu.dk

Yu Liu − *School of Mechanical Engineering and Jiangsu Key Laboratory of Advanced Food Manufacturing Equipment and Technology, Jiangnan University, Wuxi 214122, China*; orcid.org/0000-0002-7945-7462; Email: yuliu@jiangnan.edu.cn

Authors

Jun Ren − *School of Mechanical Engineering, Jiangnan University, Wuxi 214122, China*

Dongya Li − *School of Mechanical Engineering and Jiangsu Key Laboratory of Advanced Food Manufacturing Equipment and Technology, Jiangnan University, Wuxi 214122, China*; orcid.org/0000-0002-6016-4010

Wenzhen Yang − *School of Mechanical Engineering, Jiangnan University, Wuxi 214122, China*

Heng-yong Nie − *Surface Science Western, Western University, London, Ontario N6G 0J3, Canada*

Complete contact information is available at: https://pubs.acs.org/10.1021/acsaelm.1c01193

Notes

The authors declare no competing financial interest.

■ ACKNOWLEDGMENTS

This work is financially supported by National Natural Science Foundation of China (Grant 51875253).

■ REFERENCES

(1) Cai, H. H.; Wang, Y. J.; Xu, M. T.; Cheng, L.; Liu, Z. L.; Li, Z.; Dai, F. Y. Low cost, green and effective preparation of multifunctional flexible silk fabric electrode with ultra-high capacitance retention. *Carbon* **2022**, *188*, 197−208.

(2) Liang, S.; Han, Y. C.; Zhang, W. L. H.; Zhong, T. Y.; Guan, H. Y.; Song, Y. F.; Zhang, Y.; Xing, L. L.; Xue, X. Y.; Li, G. L.; Zhan, Y. p A self-powered wearable body-detecting/brain-stimulating system for improving sports endurance performance. *Nano Energy* **2022**, *93*, 106851.

(3) Wang, H.; Tao, J.; Jin, K.; Wang, X. Y.; Dong, Y. Multifunctional pressure/temperature/bending sensor made of carbon fibre-multiwall carbon nanotubes for artificial electronic application. *Compos Part a-Appl. S* **2022**, *154*, 106796.

(4) Bae, J. Y.; Gwak, E. J.; Hwang, G. S.; Hwang, H. W.; Lee, D. J.; Lee, J. S.; Joo, Y. C.; Sun, J. Y.; Jun, S. H.; Ok, M. R.; Kim, J. Y.; Kang, S. K. Biodegradable Metallic Glass for Stretchable Transient Electronics. *Adv. Sci.* **2021**, *8* (10), 2004029.

(5) Wang, Y. J.; Li, X.; Fan, S. F.; Feng, X. B.; Cao, K.; Ge, Q.; Gao, L. B.; Lu, Y. Three-Dimensional Stretchable Microelectronics by Projection Microstereolithography (P mu SL). *ACS Appl. Mater. Interfaces* **2021**, *13* (7), 8901−8908.

(6) Duan, N. M.; Shi, Z. Y.; Wang, Z. H.; Zou, B.; Zhang, C. P.; Wang, J. L.; Xi, J. R.; Zhang, X. S.; Zhang, X. Z.; Wang, G. L. Mechanically robust Ti3C2Tx MXene/Carbon fiber fabric/Thermoplastic polyurethane composite for efficient electromagnetic interference shielding applications. *Mater. Design* **2022**, *214*, 110382.

(7) Yao, Y. Y.; Jin, S. H.; Wang, M. M.; Gao, F.; Xu, B. L.; Lv, X. J.; Shu, Q. H. Mxene hybrid polyvinyl alcohol flexible composite films for electromagnetic interference shielding. *Appl. Surf. Sci.* **2022**, *578*, 152007.

(8) Lessing, J.; Glavan, A. C.; Walker, S. B.; Keplinger, C.; Lewis, J. A.; Whitesides, G. M. Inkjet printing of conductive inks with high lateral resolution on omniphobic "R(F) paper" for paper-based electronics and MEMS. *Adv. Mater.* **2014**, *26* (27), 4677−4682.

(9) Shahariar, H.; Kim, I.; Soewardiman, H.; Jur, J. S. Inkjet Printing of Reactive Silver Ink on Textiles. *ACS Appl. Mater. Interfaces* **2019**, *11* (6), 6208−6216.

(10) Zhou, H. H.; Song, Y. L. Fabrication of Silver Mesh/Grid and Its Applications in Electronics. *ACS Appl. Mater. Interfaces* **2021**, *13* (3), 3493−3511.

(11) Garcia, A.; Polesel-Maris, J.; Viel, P.; Palacin, S.; Berthelot, T. Localized Ligand Induced Electroless Plating (LIEP) Process for the

Fabrication of Copper Patterns Onto Flexible Polymer Substrates. *Adv. Funct Mater.* **2011**, *21* (11), 2096−2102.
(12) Hu, J.; Yu, M. F. Meniscus-Confined Three-Dimensional Electrodeposition for Direct Writing of Wire Bonds. *Science* **2010**, *329* (5989), 313−316.
(13) Nam, K. H.; Abdulhafez, M.; Castagnola, E.; Tomaraei, G. N.; Cui, X. T.; Bedewy, M. Laser direct write of heteroatom-doped graphene on molecularly controlled polyimides for electrochemical biosensors with nanomolar sensitivity. *Carbon* **2022**, *188*, 209−219.
(14) Abubakr, E.; Ohmagari, S.; Zkria, A.; Ikenoue, H.; Yoshitake, T. Laser-induced novel ohmic contact formation for effective charge collection in diamond detectors. *Mat Sci. Semicon Proc.* **2022**, *139*, 106370.
(15) Museur, L.; Manousaki, A.; Anglos, D.; Tsibidis, G. D.; Kanaev, A. Pathways control in modification of solid surfaces induced by temporarily separated femtosecond laser pulses. *Appl. Surf. Sci.* **2021**, *566*, 150611.
(16) Lin, C. W.; Hsieh, P. Y.; Chou, C. M.; Chung, C. J.; He, J. L. Femtosecond laser surface roughening and pulsed plasma polymerization duplex treatment on medical-grade stainless steel substrates for orthodontic purpose. *Surf. Coat. Technol.* **2021**, *427*, 127819.
(17) Sharma, B.; Sharma, A. Enhanced surface dynamics and magnetic switching of alpha-Fe2O3 films prepared by laser assisted chemical vapor deposition. *Appl. Surf. Sci.* **2021**, *567*, 150724.
(18) Da Silva, A.; Frostevarg, J.; Volpp, J.; Kaplan, A. F. H. Additive Manufacturing by laser-assisted drop deposition from a metal wire. *Mater. Design* **2021**, *209*, 109987.
(19) Shen, H. J.; Wang, Y. D.; Cao, L.; Xie, Y.; Wang, L.; Chu, X. Y.; Shi, K. X.; Wang, S. Z.; Yu, M. M.; Liu, R.; Zhang, J. R.; Li, C. L.; Weng, Z. K.; Wang, Z. B. Fabrication of periodic microscale stripes of silver by laser interference induced forward transfer and their SERS properties. *Nanotechnology* **2022**, *33* (11), 115302.
(20) Zhang, J. F.; Liu, Y. X.; Ronneberger, S.; Tarakina, N. V.; Merbouh, N.; Loeffler, F. F. Nanolayer Laser Absorber for Femtoliter Chemistry in Polymer Reactors. *Adv. Mater.* **2022**, *34*, 2108493.
(21) Liang, J. J.; Chen, Y. S.; Xu, Y. F.; Liu, Z. B.; Zhang, L.; Zhao, X.; Zhang, X. L.; Tian, J. G.; Huang, Y.; Ma, Y. F.; Li, F. F. Toward All-Carbon Electronics: Fabrication of Graphene-Based Flexible Electronic Circuits and Memory Cards Using Maskless Laser Direct Writing. *ACS Appl. Mater. Interfaces* **2010**, *2* (11), 3310−3317.
(22) Yang, C.; Cui, X. Y.; Zhang, Z. X.; Chiang, S. W.; Lin, W.; Duan, H.; Li, J.; Kang, F. Y.; Wong, C. P. Fractal dendrite-based electrically conductive composites for laser-scribed flexible circuits. *Nat. Commun.* **2015**, *6*, 8150.
(23) Wang, J.; Chen, H.; Zhao, Y.; Zhong, Z. B.; Tang, Y.; Liu, G. Z.; Feng, X.; Xu, F. C.; Chen, X. H.; Cai, D. J.; Kang, J. Y. Programmed Ultrafast Scan Welding of Cu Nanowire Networks with a Pulsed Ultraviolet Laser Beam for Transparent Conductive Electrodes and Flexible Circuits. *ACS Appl. Mater. Interfaces* **2020**, *12* (31), 35211−35221.
(24) Zakhidov, A. A.; Fong, H. H.; DeFranco, J. A.; Lee, J. K.; Taylor, P. G.; Ober, C. K.; Malliaras, G. G.; He, M. Q.; Kane, M. G. Fabrication of polymer-based electronic circuits using photolithography. *Appl. Phys. Lett.* **2011**, *99* (18), 183308.
(25) Yang, J. U.; Cho, J. H.; Yoo, M. J. Selective metallization on copper aluminate composite via laser direct structuring technology. *Compos Part B-Eng.* **2017**, *110*, 361−367.
(26) Zhang, J.; Zhou, T.; Wen, L. Selective Metallization Induced by Laser Activation: Fabricating Metallized Patterns on Polymer via Metal Oxide Composite. *ACS Appl. Mater. Interfaces* **2017**, *9* (10), 8996−9005.
(27) Zhang, J. H.; Feng, J.; Jia, L. Y.; Zhang, H. Y.; Zhang, G. X.; Sun, S. H.; Zhou, T. Laser-Induced Selective Metallization on Polymer Substrates Using Organocopper for Portable Electronics. *ACS Appl. Mater. Interfaces* **2019**, *11* (14), 13714−13723.
(28) Zhang, Y.; Hansen, H. N.; De Grave, A.; Tang, P. T.; Nielsen, J. S. Selective metallization of polymers using laser induced surface activation (LISA)-characterization and optimization of porous surface topography. *Int. J. Adv. Manuf Tech* **2011**, *55* (5−8), 573−580.
(29) Zhang, Y.; Kontogeorgis, G. M.; Hansen, H. N. An Explanation of the Selective Plating of Laser Machined Surfaces Using Surface Tension Components. *J. Adhes Sci. Technol.* **2011**, *25* (16), 2101−2111.
(30) Zhang, Y.; Hansen, H. N.; Tang, P. T.; Nielsen, J. S. Verification of a characterization method of the laser-induced selective activation based on industrial lasers. *Int. J. Adv. Manuf Tech* **2013**, *68* (9), 1775−1783.
(31) Lee, J. H.; Youn, D. Y.; Luo, Z.; Moon, J. Y.; Choi, S. J.; Kim, C.; Kim, I. D. Cu Microbelt Network Embedded in Colorless Polyimide Substrate: Flexible Heater Platform with High Optical Transparency and Superior Mechanical Stability. *ACS Appl. Mater. Interfaces* **2017**, *9* (45), 39650−39656.
(32) Chen, J. J.; An, Q.; Rodriguez, R. D.; Sheremet, E.; Wang, Y.; Sowade, E.; Baumann, R. R.; Feng, Z. S. Surface modification with special morphology for the metallization of polyimide film. *Appl. Surf. Sci.* **2019**, *487*, 503−509.
(33) Li, Y.; Lu, Q. H.; Qian, X. F.; Zhu, Z. K.; Yin, J. Preparation of surface bound silver nanoparticles on polyimide by surface modification method and its application on electroless metal deposition. *Appl. Surf. Sci.* **2004**, *233* (1−4), 299−306.
(34) Liao, Y. C.; Kao, Z. K. Direct writing patterns for electroless plated copper thin film on plastic substrates. *ACS Appl. Mater. Interfaces* **2012**, *4* (10), 5109−5113.
(35) Zhang, Y. B.; Zhang, T.; Shi, H. B.; Liu, Q.; Shi, Y. L.; Wang, T. Electroless Plating Cycle Process for High-Conductivity Flexible Printed Circuits. *Acs Sustain Chem. Eng.* **2021**, *9* (35), 11991−12004.
(36) Wang, P. C.; Liu, Y. M.; Chang, C. P.; Liao, Y. Y.; Peng, Y. Y.; Ger, M. D. A laser curable palladium complex ink used for fabrication of copper pattern on polyimide substrate. *J. Taiwan Inst Chem. E* **2017**, *80*, 963−969.
(37) Zhai, T.; Ding, C. H.; Lu, L. X.; Zhang, C.; Yang, D. A. Autocatalytic deposition of copper coating on poly (ether ether ketone)/multiwalled carbon nanotubes composites via a palladium-free and simplified electroless process. *Mater. Lett.* **2015**, *147*, 46−49.
(38) Huang, J.; Tian, C.; Wang, J.; Liu, J.; Li, Y.; Liu, Y.; Chen, Z. Fabrication of selective electroless copper plating on PET sheet: Effect of PET surface structure on resolution and adhesion of copper coating. *Appl. Surf. Sci.* **2018**, *458*, 734−742.
(39) Zhang, Y.; Zhang, T.; Shi, H.; Liu, Q.; Wang, T. Fabrication of flexible copper patterns by electroless plating with copper nanoparticles as seeds. *Appl. Surf. Sci.* **2021**, *547*, 149220.
(40) Marla, D.; Andersen, S. A.; Zhang, Y.; Hattel, J. H.; Spangenberg, J. A study of laser surface modification of polymers: A comparison in air and water. *J. Manuf Process* **2018**, *32* (4), 432−437.
(41) Marla, D.; Zhang, Y.; Hattel, J. H.; Spangenberg, J. Modeling of nanosecond pulsed laser processing of polymers in air and water. *Model Simul Mater. Sc* **2018**, *26* (5), No. 055005.
(42) Marla, D.; Zhang, Y.; Jabbari, M.; Sonne, M. R.; Spangenberg, J.; Hattel, J. H. A computational model for heterogeneous heating during pulsed laser irradiation of polymers doped with light-absorbing microparticles. *Appl. Phys. a-Mater.* **2016**, *122* (12), 1042−1051.
(43) Aktinol, E.; Dhir, V. K. Numerical Simulation of Nucleate Boiling Phenomenon Coupled with Thermal Response of the Solid. *Microgravity Sci. Tec* **2012**, *24* (4), 255−265.
(44) Ling, K.; Tao, W. Q. Numerical simulation of nucleate boiling in shallow liquid. *Comput. Fluids* **2018**, *164* (3), 35−40.
(45) Huang, G. H.; Li, W. M.; Ma, J. X.; Ren, C. C.; Li, C. High-frequency alternating nucleate boiling of water enabled by microslot arrays in microchannels. *Int. J. Heat Mass Tran* **2020**, *150*, 119271.
(46) Zaksek, P.; Zupancic, M.; Gregorcic, P.; Golobic, I. Investigation of Nucleate Pool Boiling of Saturated Pure Liquids and Ethanol-Water Mixtures on Smooth and Laser-Textured Surfaces. *Nanosc Microsc Therm* **2020**, *24* (1), 29−42.
(47) Holopainen, S. Modeling of the mechanical behavior of amorphous glassy polymers under variable loadings and comparison with state-of-the-art model predictions. *Mech Mater.* **2013**, *66*, 35−58.
(48) ASTM International. *Standard Test Method for Measuring Adhesion by Tape Test*; ASTM D3359-09; ASTM: West Conshohocken, PA, 2010. DOI: 10.1520/D3359-09E02.

(49) Zhang, Q.; Zhou, W. Y.; Xia, X. G.; Li, K. W.; Zhang, N.; Wang, Y. C.; Xiao, Z. J.; Fan, Q. X.; Kauppinen, E. I.; Xie, S. S. Transparent and Freestanding Single-Walled Carbon Nanotube Films Synthesized Directly and Continuously via a Blown Aerosol Technique. *Adv. Mater.* **2020**, *32* (39), 2004277.
(50) Jensen, B. D.; Huang, K.; Chow, L. L. W.; Kurabayashi, K. Low-force contact heating and softening using micromechanical switches in diffusive-ballistic electron-transport transition. *Appl. Phys. Lett.* **2005**, *86* (2), No. 023507.
(51) Samet, D.; Rambhatla, V. N. N. T.; Kwatra, A.; Sitaraman, S. K. A fatigue crack propagation model with resistance curve effects for an epoxy/copper interface. *Eng. Fract Mech* **2017**, *180*, 60−72.
(52) Wanasinghe, D.; Aslani, F. A review on recent advancement of electromagnetic interference shielding novel metallic materials and processes. *Compos Part B-Eng.* **2019**, *176* (11), 107207.
(53) Guo, H. T.; Chen, Y. M.; Li, Y.; Zhou, W.; Xu, W. H.; Pang, L.; Fan, X. M.; Jiang, S. H. Electrospun fibrous materials and their applications for electromagnetic interference shielding: A review. *Compos Part a-Appl. S* **2021**, *143* (6), 1359−1376.

https://doi.org/10.1021/acsaelm.1c01193
ACS Appl. Electron. Mater. 2022, 4, 2191−2202